Mark Erickson
Graduate Research Assistant

Mark Costello
Assistant Professor

Department of Mechanical Engineering,
Oregon State University,
Corvallis, OR 97331

Production Line Calibration for Sensors on Actively Controlled Bullets

A simple testing device is presented that simultaneously calibrates all dominant error sources for accelerometers and gyroscopes found in typical microelectromechanical inertial measurement units on smart projectiles, including bias, scale factor, cross axis sensitivity/misalignment, and misposition. The device consists of a table which rotates about a gimbal joint and is supported on the corners by elastic and damping elements. Using dynamic simulation it is shown that motion created by free vibration of the testing platform suitably excites sensors on projectiles so calibration can be performed. Calibration parameters are estimated using an extended Kalman filter. Platform support stiffness and damping characteristics significantly alter the time required to identify calibration parameters by shaping platform motion. A critical level of initial motion of the testing platform is required for adequate prediction of calibration parameters.
[DOI: 10.1115/1.1688376]

Introduction

Insertion of active control technology into medium and small caliber gun launched bullets offers the possibility to increase the lethality of these weapons by an order of magnitude. Fundamentally, actively controlled projectiles greatly reduce shot-to-shot target impact point dispersion, allowing targets to be engaged at longer ranges while maintaining the same probability of kill. While the potential of active control technology applied to gun launched munitions is enormous, equally daunting challenges must be surmounted. Gun launched bullets are exposed to a harsh environment, particularly at launch where large accelerations are experienced. In this environment, the sensors, control mechanism, and associated electronics must be rugged. Furthermore, bullets are relatively small objects and physical space requirements for the flight control system must be minimized to maintain target effects generated by the munition. Practical implementation of actively controlled medium and small caliber projectiles into the arsenal will be driven not only by flight performance but also by system cost. Significant cost advantages are attained by employing inexpensive sensors in the flight control system, yielding conconsumately less accurate devices.

In order to increase the accuracy of individual sensors, error sources such as bias, scale factor, and cross axis sensitivity can be experimentally determined by exciting the sensor and contrasting the results against a known source. For example, Tustin [1] discusses common techniques for obtaining the scale factor of an accelerometer. McConnell and Han [2] as well as Witter and Brown [3] considered calibration of accelerometers mounted on a rigid beam. Cross axis sensitivity of each sensor was estimated using frequency response methods. Boutillon and Faure [4] developed the mean projection method for cross axis sensitivity estimation of accelerometers using standard vibration shakers. Sutton [5] as well as Payne and Evens [6] considered accelerometer calibration using laser interferometry. Gabrielson [7] reported a technique to calibrate accelerometers and velocity sensors using a simple fixture and 2 geophones. Sensor errors can also be generated by improper placement and orientation of sensors on the parent body. These types of errors can be reduced by exciting the sensors that are mounted on the body and contrasting the measurements against a known source. Grewal [8] considered calibration and alignment of an inertial measurement unit using Kalman filtering. The basic inertial measurement unit (IMU) dynamic equations are augmented with state equations to predict unknown sensor parameters, so that sensor errors can be estimated and corrected in real time. Later, Kong, Nebot, and Durrant-Whyte [9] developed an inertial navigation system alignment and calibration method capable of estimating large misalignment of sensors.

The work documented here establishes a relatively simple device and associated data processing that identifies and calibrates all the major error sources of a sensor suite onboard a smart projectile. For IMU type sensor suites, this includes identification of accelerometer scale factor, bias, cross axis sensitivity, and misposition for all three single axis accelerometers as well as gyroscope scale factor, bias, and cross axis sensitivity for all three single axis gyroscopes. The calibration device accommodates many projectiles simultaneously so that it can be used in a high production rate manufacturing system as one of the last operations on the production line.

Calibration Device

Figure 1 provides a sketch of the calibration device. The calibration platform consists of a rigid table supported at each corner by elastic elements. The center of the table is fixed to a gimbal joint, therefore limiting the platform to 3 rotation degrees of freedom. Limiting the platform to 3 degrees of freedom greatly reduces the complexity of the position and orientation measurement system which in turn reduces measurement errors that adversely affect calibration accuracy. The calibration platform is a passive system, meaning the necessary motion is obtained by deflecting the platform from its equilibrium state in such a fashion to excite sufficient motion in free vibration. Elastic element properties are tuned to minimize parameter estimation time. The table surface consists of numerous projectile mounting fixtures which allow for quick and precise fastening of a large quantity of rounds onto the fixture that is necessary for a high production rate manufacturing environment. Each mounting fixture secures the bullet in a unique orientation and position such that the distance vector between the table pivot point and the mass center of the bullet is established with high precision. In addition, three angular potentiometers are mounted at the gimbal joint. These potentiometers provide the platform Euler orientation angles and when differentiated, angular velocity and angular acceleration. With this information, platform kinematics are determined and provide a basis for obtaining acceleration and angular rates at each sensor point. Sensor data from

Contributed by the Manufacturing Engineering Division for publication in the JOURNAL OF MANUFACTURING SCIENCE AND ENGINEERING. Manuscript received May 2002; Revised December 2003. Associate Editor: K. Danai.

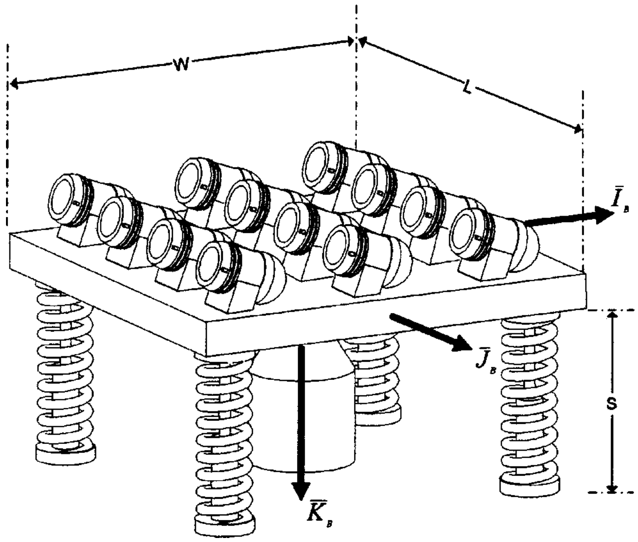

Fig. 1 Schematic of sensor calibration device

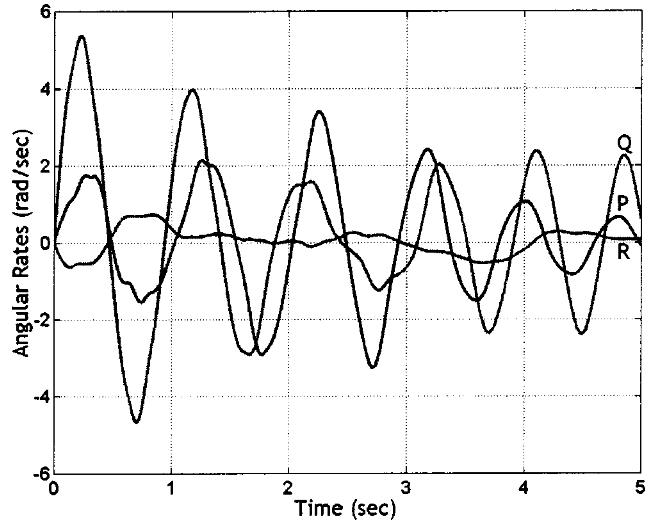

Fig. 3 Angular velocity of calibration platform

the IMU of each bullet is obtained through a wiring harness connected directly to each bullet. Relative to the onboard projectile sensors, the platform sensors are very accurate and in this work assumed ideal.

Dynamic Model of Vibrating Platform

Performance of the sensor calibration system is analyzed using dynamic simulation. The calibration device dynamics are modeled as a rigid body with 3 rotational degrees of freedom [10] The orientation of a body element is defined by a sequence of three body fixed Euler angle rotations. Starting from the inertial reference frame a rotation of ψ is executed about the $\vec{K}_I$ axis. The resulting rotated reference frame is called the O frame. Next, the O frame is rotated about the $\vec{J}_O$ axis by the angle θ. The resulting reference frame is denoted the T frame. The T frame is subsequently rotated about the $\vec{I}_T$ axis by the angle ϕ yielding the body reference frame. The angles ϕ, θ, and ψ are the Euler angles associated with the body. The angular velocity of the body can be written in terms of Euler angle time derivatives,

$$\vec{\omega}_{B/I}=\dot{\phi}\vec{I}_T+\dot{\theta}\vec{J}_O+\dot{\psi}\vec{K}_I \tag{1}$$

or in terms of the calibration platform reference frame angular velocity components.

$$\vec{\omega}_{B/I}=p\vec{I}_B+q\vec{J}_B+r\vec{K}_B \tag{2}$$

The kinematic relationship between time derivatives of the Euler angles from Eq. (1) and body frame angular velocity components in Eq. (2) is shown in Eq. (3).

$$\begin{Bmatrix} \dot{\phi} \\ \dot{\theta} \\ \dot{\psi} \end{Bmatrix} = \begin{bmatrix} 1 & s_\phi t_\theta & c_\phi \\ 0 & c_\phi & -s_\phi \\ 0 & s_\phi/c_\theta & c_\phi/c_\theta \end{bmatrix} \begin{Bmatrix} p \\ q \\ r \end{Bmatrix} \tag{3}$$

Equation (3) uses the following shorthand notation for trigonometric sine, cosine, and tangent functions: $s_\alpha \equiv \sin\alpha$, $c_\alpha \equiv \cos\alpha$, $t_\alpha \equiv \tan\alpha$. The rotational dynamic equation for the calibration platform is achieved by setting the total applied moment on the platform about the platform mass center equal to the time rate of change of the angular momentum of the platform. Equation (4) describes this equation with components in the platform reference frame.

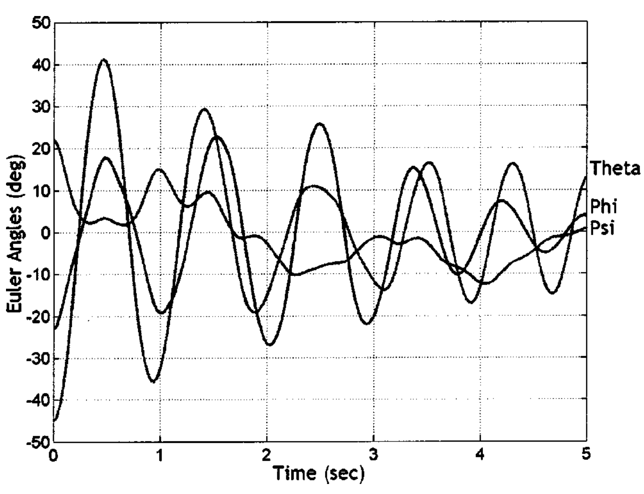

Fig. 2 Orientation of calibration platform

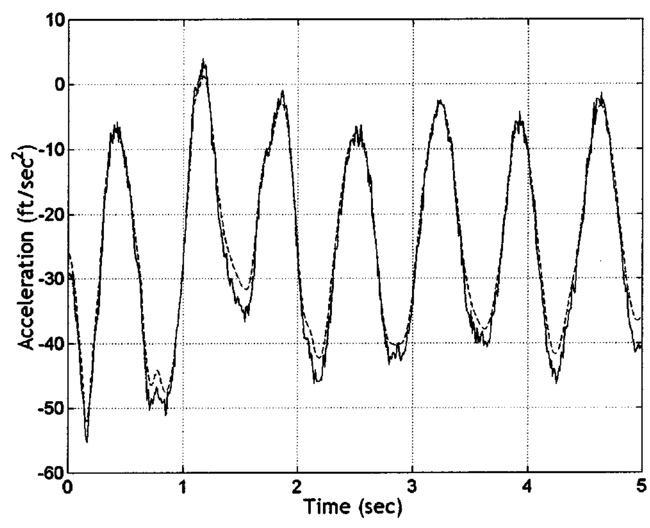

Fig. 4 Accelerometer signal vs. time. (solid line = accelerometer reading, dashed line = kinematically construction acceleration)

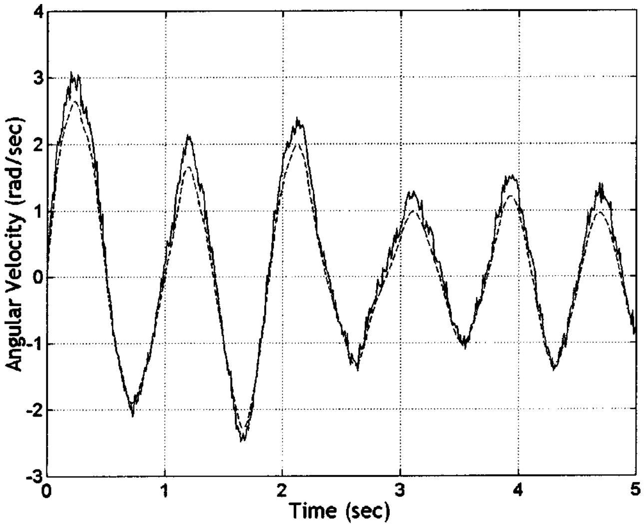

Fig. 5 Gyroscope signal vs. time (solid line=gyroscope reading, dashed line=kinematically constructed angular velocity)

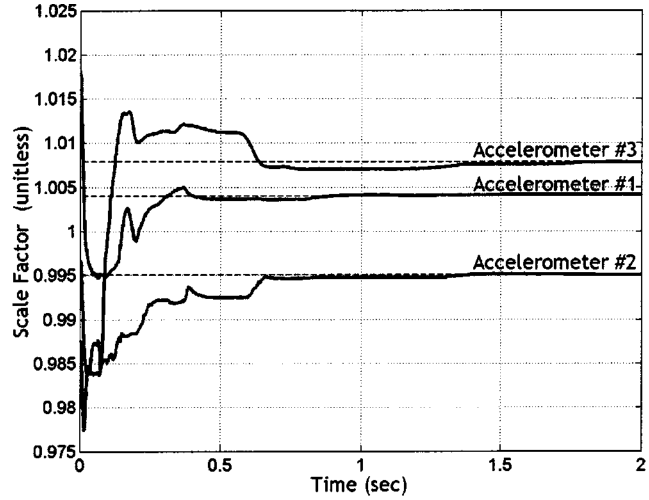

Fig. 7 Accelerometer scale factor parameter estimates vs. time (solid line=estimate, dashed line=kinematically constructed value)

$$\begin{Bmatrix} \dot{p} \\ \dot{q} \\ \dot{r} \end{Bmatrix} = [I]^{-1}\left(\begin{Bmatrix} L \\ M \\ N \end{Bmatrix} - \begin{bmatrix} 0 & -r & q \\ r & 0 & -p \\ -q & p & 0 \end{bmatrix} [I] \begin{Bmatrix} p \\ q \\ r \end{Bmatrix} \right) \tag{4}$$

In Eq. (4), I denotes the mass moment of inertia matrix of the calibration platform about its own mass center. Also in Eq. (4), L,M,N represent the components of the total externally applied moment vector on the body about its own mass center expressed in its own reference frame. The applied moments about the mass center of the table are caused by gimbal joint reaction forces and elastic support loads.

$$\begin{Bmatrix} L \\ M \\ N \end{Bmatrix} = \begin{Bmatrix} L_S \\ M_S \\ N_S \end{Bmatrix} + \begin{Bmatrix} L_D \\ M_D \\ N_D \end{Bmatrix} + \begin{Bmatrix} L_R \\ M_R \\ N_R \end{Bmatrix} \tag{5}$$

The applied moment component due to spring forces is computed by crossing the distance vector from the platform mass center to the spring attachment point with the spring force vector.

$$\begin{Bmatrix} L_S \\ M_S \\ N_S \end{Bmatrix} = \sum_{k=1}^{N} \begin{bmatrix} 0 & z_{\oplus}-z_{c_k} & y_{c_k}-y_{\oplus} \\ z_{c_k}-z_{\oplus} & 0 & x_{\oplus}-x_{c_k} \\ y_{\oplus}-y_{c_k} & x_{c_k}-x_{\oplus} & 0 \end{bmatrix} \begin{Bmatrix} X_{S_k} \\ Y_{S_k} \\ Z_{S_k} \end{Bmatrix} \tag{6}$$

The spring force vector is determined by multiplying the spring stiffness by the change in length of the spring and aligning this force along the unit vector $\overline{e_i}$ pointing from the floor connection point to the table corner.

$$\begin{Bmatrix} X_{S_k} \\ Y_{S_k} \\ Z_{S_k} \end{Bmatrix} = k_k \ \Delta s_k \begin{Bmatrix} e_{x_k} \\ e_{y_k} \\ e_{z_k} \end{Bmatrix} \tag{7}$$

where:

$$\vec{e}_k = \frac{\vec{r}_{F_k \to T_k}}{|\vec{r}_{F_k \to T_k}|} = e_{x_k}\overline{I_I} + e_{y_k}\overline{J_I} + e_{z_k}\overline{K_I} \tag{8}$$

$$\Delta s = s_o - |\vec{r}_{F_k \to T_k}| \tag{9}$$

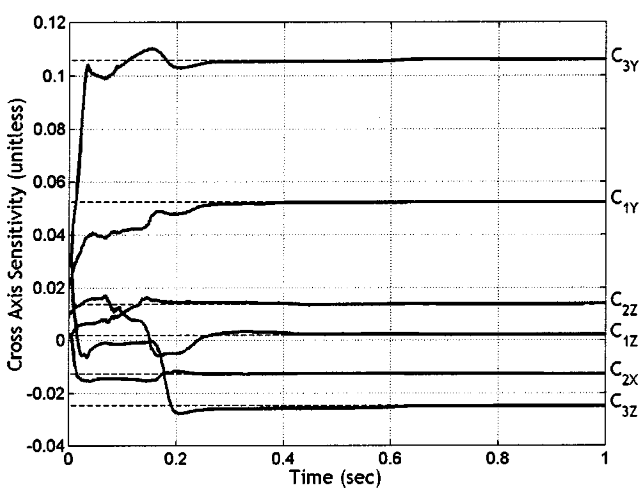

Fig. 6 Accelerometer cross axis sensitivity parameter estimates vs. time (solid line=estimate, dashed line =kinematically constructed value)

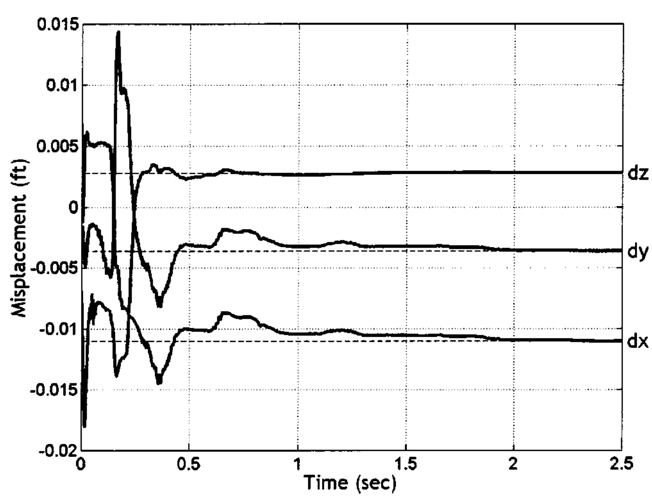

Fig. 8 Accelerometer #1 misposition parameter estimates vs. time (solid line=estimate, dashed line=kinematically constructed value)

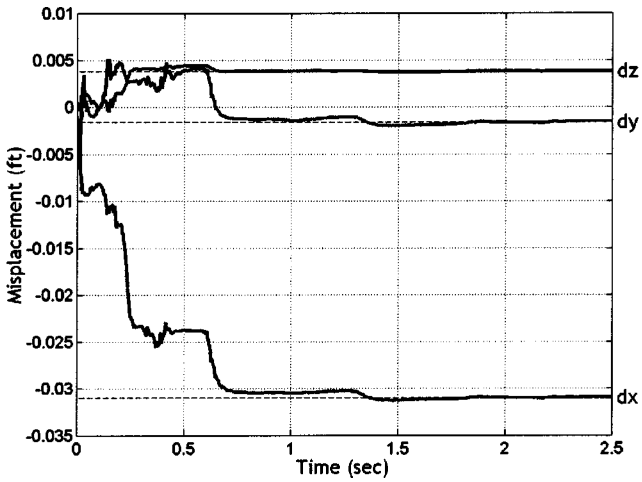

Fig. 9 Accelerometer #2 misposition parameter estimates vs. time (solid line=estimate, dashed line=kinematically constructed value)

The moment components resulting from the effect of the four dampers are determined in the same fashion as the springs.

$$\begin{Bmatrix} L_D \\ M_D \\ N_D \end{Bmatrix} = \sum_{k=1}^{N} c_k \dot{s}_k \begin{bmatrix} 0 & z_{\oplus} - z_{c_k} & y_{c_k} - y_{\oplus} \\ z_{c_k} - z_{\oplus} & 0 & x_{\oplus} - x_{c_k} \\ y_{\oplus} - y_{c_k} & x_{c_k} - x_{\oplus} & 0 \end{bmatrix} \begin{Bmatrix} X_{D_k} \\ Y_{D_k} \\ Z_{D_k} \end{Bmatrix} \tag{10}$$

Where the damper force vector is given as:

$$\begin{Bmatrix} X_{D_k} \\ Y_{D_k} \\ Z_{D_k} \end{Bmatrix} = c_k \dot{s}_k \begin{Bmatrix} e_{x_k} \\ e_{y_k} \\ e_{z_k} \end{Bmatrix} \tag{11}$$

The moment due to the reaction force located at the gimbal joint is computed according to

$$\begin{Bmatrix} L_D \\ M_D \\ N_D \end{Bmatrix} = \begin{bmatrix} 0 & z_{\oplus} - z_P & y_P - y_{\oplus} \\ z_P - z_{\oplus} & 0 & x_{\oplus} - x_P \\ y_{\oplus} - y_P & x_P - x_{\oplus} & 0 \end{bmatrix} \begin{Bmatrix} X_R \\ Y_R \\ Z_R \end{Bmatrix} \tag{12}$$

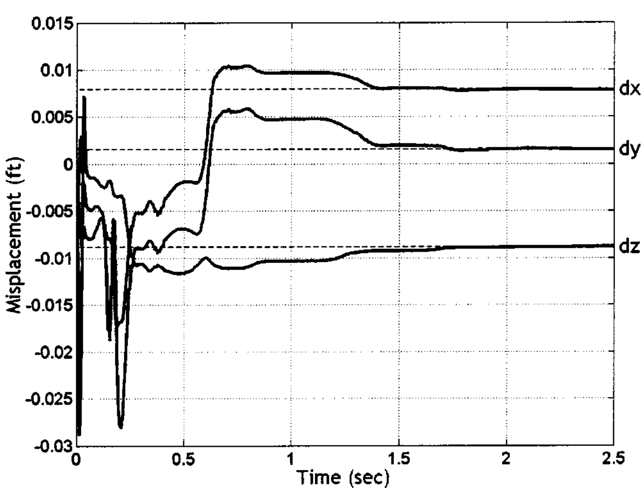

Fig. 10 Accelerometer #3 misposition parameter estimates vs. time (solid line=estimate, dashed line=kinematically constructed value)

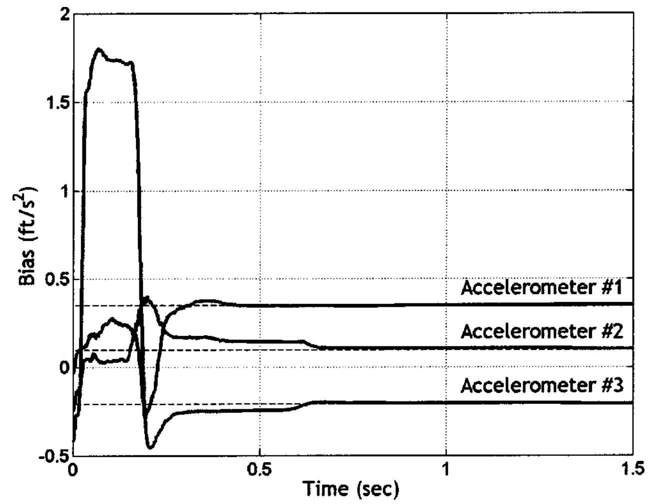

Fig. 11 Accelerometer bias parameter estimates vs. time (solid line=estimate, dashed line=kinematically constructed value)

The gimbal joint reactions are computed using the translational dynamic equations

$$\begin{Bmatrix} X_R \\ Y_R \\ Z_R \end{Bmatrix} = m \begin{Bmatrix} a_{\oplus_X} \\ a_{\oplus_Y} \\ a_{\oplus_Z} \end{Bmatrix} - m\vec{g} - \sum_{k=1}^{4} \begin{Bmatrix} X_{S_k} \\ Y_{S_k} \\ Z_{S_k} \end{Bmatrix} - \sum_{k=1}^{4} \begin{Bmatrix} X_{D_k} \\ Y_{D_k} \\ Z_{D_k} \end{Bmatrix} \tag{13}$$

where the mass center acceleration can be written as:

$$\begin{Bmatrix} a_{\oplus_X} \\ a_{\oplus_Y} \\ a_{\oplus_Z} \end{Bmatrix} = [S_\alpha + S_\omega S_\omega] \begin{Bmatrix} x_{\oplus} - x_P \\ y_{\oplus} - y_P \\ z_{\oplus} - z_P \end{Bmatrix} = [S] \begin{Bmatrix} x_{\oplus} - x_P \\ y_{\oplus} - y_P \\ z_{\oplus} - z_P \end{Bmatrix} \tag{14}$$

$$\text{where:} \qquad S_\omega = \begin{bmatrix} 0 & -r & q \\ r & 0 & -p \\ -q & p & 0 \end{bmatrix}$$

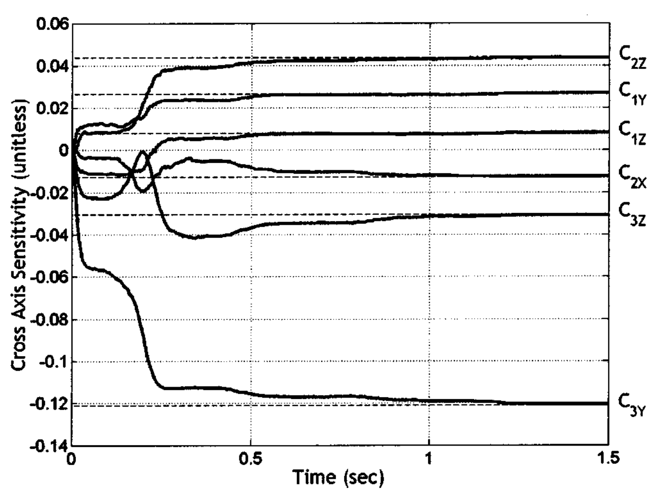

Fig. 12 Gyroscope cross axis sensitivity parameter estimates vs. time (solid line=estimate, dashed line=kinematically constructed value)

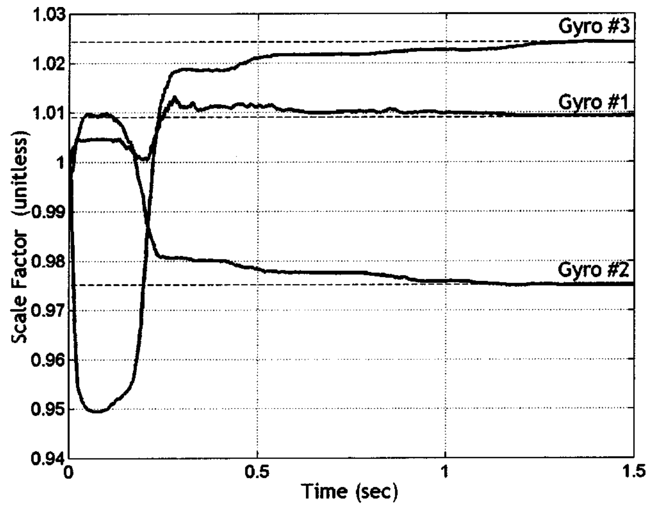

Fig. 13 Gyroscope scale factor parameter estimates vs. time (solid line=estimate, dashed line=kinematically constructed value)

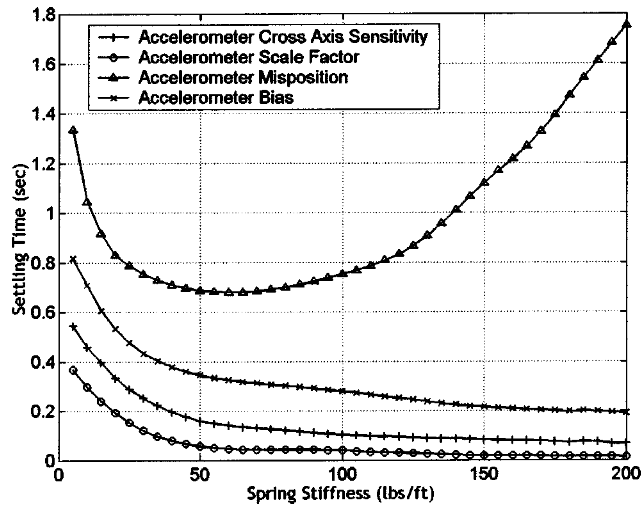

Fig. 15 Accelerometer Parameter Settling Time vs. Spring Stiffness.

$$S_\alpha = \begin{bmatrix} 0 & -\dot{r} & \dot{q} \\ \dot{r} & 0 & -\dot{p} \\ -\dot{q} & \dot{p} & 0 \end{bmatrix}$$

Equation (14) incorporates the fact that the acceleration of the gimbal point is zero.

The dynamic model of the 3 degree of freedom vibrating platform yields a set of six first order differential equations of motion which are integrated forward in time using a fourth order Runge-Kutta method to predict ϕ, θ, ψ, p, q, and r. Kinematic equations are subsequently used to determine acceleration at any point on the table corresponding to sensor locations. In order to simulate actual sensor readings, the sensors are mispositioned and bias, scale factor and cross axis sensitivity/misalignment errors along with noise are superimposed on the simulation sensor data. These two sets of data are used to investigate the calibration procedure.

Single Axis Accelerometer Model

Each projectile is rigidly mounted on the calibration platform. Likewise, each projectile has 3 single axis accelerometers rigidly mounted to the projectile. Description of the sensed acceleration of the ith accelerometer is aided by the A_i reference frame that has its origin located at the sensor point and the $\overline{I_{A_i}}$ axis aligned with the sensitive axis of the ith accelerometer. The ith accelerometer and body reference frames are related by

$$\begin{Bmatrix} \overline{I_{S_i}} \\ \overline{J_{S_i}} \\ \overline{K_{S_i}} \end{Bmatrix} = [T_{A_i}] \begin{Bmatrix} \overline{I_B} \\ \overline{J_B} \\ \overline{K_B} \end{Bmatrix} \tag{15}$$

The acceleration of the point where the ith accelerometer is mounted expressed in the ith accelerometer reference frame is given by:

$$\begin{Bmatrix} a_{x_i} \\ a_{y_i} \\ a_{z_i} \end{Bmatrix} = [S_\alpha + S_\omega S_\omega] \begin{Bmatrix} x_P - x_{Ai} \\ y_P - y_{A_i} \\ z_P - z_{A_i} \end{Bmatrix} \tag{16}$$

Readings obtained by an accelerometer are corrupted by noise, bias errors, cross axis sensitivity, scale factor error, and misposition. Because accelerometers record gravitational loads, the effect

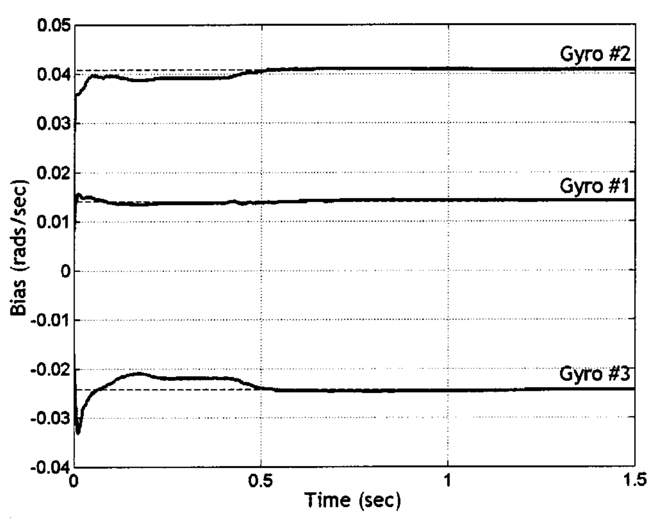

Fig. 14 Gyroscope bias parameter estimates vs. time (solid line=estimate, dashed line=kinematically constructed value)

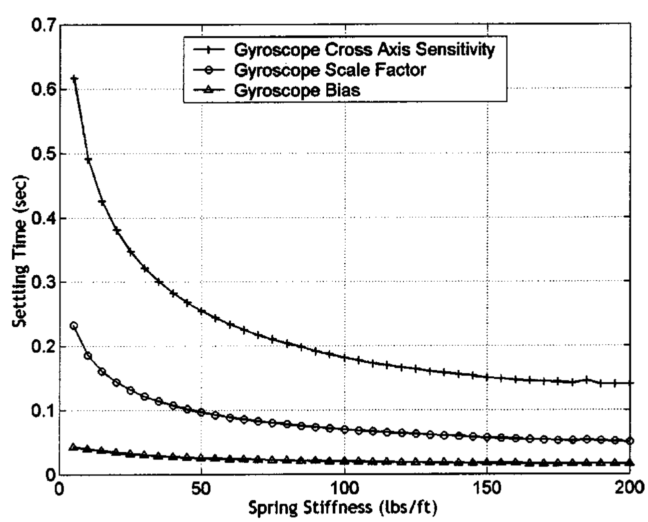

Fig. 16 Gyroscope Parameter Settling Time vs. Spring Stiffness.

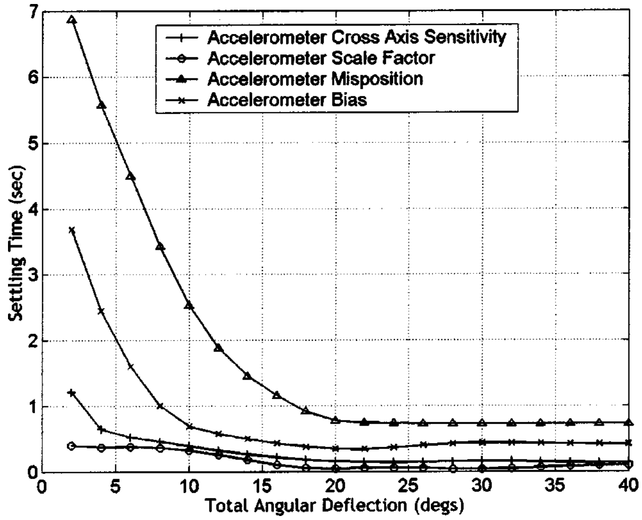

Fig. 17 Accelerometer Parameter Settling Time vs. Magnitude of Initial Motion.

of gravity is also present in the readings. Thus, the sensed readings by the i[th] accelerometer can be described by:

$$a_i = a_{N_i} + a_{B_i} + [S_{A_i}\ \ C^y_{A_i}\ \ C^z_{A_i}][T_{A_i}] \times \left[[S_\alpha + S_\omega S_\omega] \begin{Bmatrix} x_P - x_{A_i} - \delta x_i \\ y_P - y_{A_i} - \delta y_i \\ z_P - z_{A_i} - \delta z_i \end{Bmatrix} - g \begin{Bmatrix} -s_\theta \\ s_\phi c_\theta \\ c_\phi c_\theta \end{Bmatrix} \right] \quad (17)$$

For purposes of global calibration, cross axis sensitivity and misalignment of the sensor create the same effect on sensor readings, however only cross axis sensitivity effects are included in the model above. Thus, identified cross axis sensitivity includes sensor misalignment.

On a body with one point fixed, the effect of scaling an acceleration measurement and the effect of misplacing an accelerometer are indistinguishable. To see this, express the acceleration components in a reference frame where the $\overline{I}$ axis is aligned with the misposition vector.

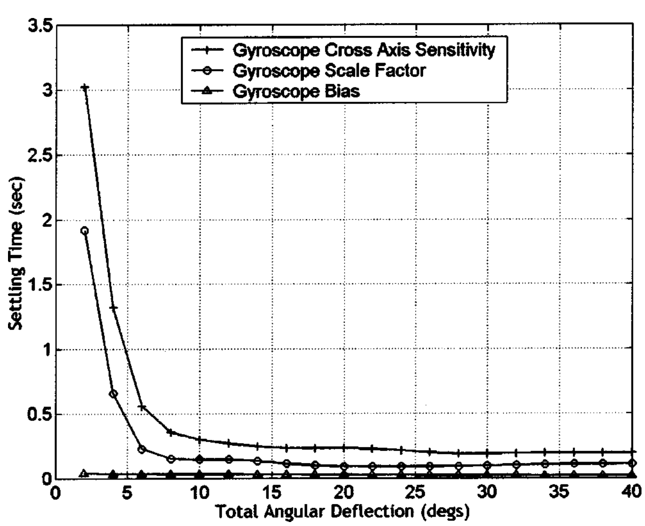

Fig. 18 Gyroscope Parameter Settling Time vs. Magnitude of Initial Motion.

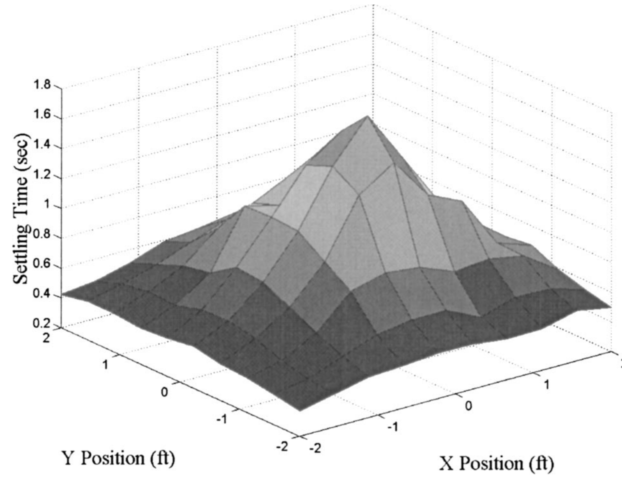

Fig. 19 Accelerometer Cross Axis Sensitivity Parameter Settling Time vs. Projectile Mounting Position.

$$\begin{Bmatrix} a_{x_{MP}} \\ a_{y_{MP}} \\ a_{z_{MP}} \end{Bmatrix} = \begin{Bmatrix} a_{x_i} \\ a_{y_i} \\ a_{z_i} \end{Bmatrix} + [S] \begin{Bmatrix} \Delta x_{MP} \\ 0 \\ 0 \end{Bmatrix} = \begin{Bmatrix} a_{x_i} \\ a_{y_i} \\ a_{z_i} \end{Bmatrix} + \Delta x_{MP} \begin{Bmatrix} S_{11} \\ S_{21} \\ S_{31} \end{Bmatrix} \quad (18)$$

Also, express the scale factor as unity plus a factor, s_i^A.

$$\begin{Bmatrix} a_{x_{SF}} \\ a_{y_{SF}} \\ a_{z_{SF}} \end{Bmatrix} = \begin{Bmatrix} a_{x_i} \\ a_{y_i} \\ a_{z_i} \end{Bmatrix} + s_i^A \begin{Bmatrix} a_{x_i} \\ a_{y_i} \\ a_{z_i} \end{Bmatrix} \quad (19)$$

For single axis accelerometers, the measurement with misposition error is a linear combination of the measurement with scale factor error leading to both calibration parameters modifying the sensed acceleration in a linear fashion. However, when motion is caused by translation and rotation of the body or the sensor registers translational acceleration, as is the case for an accelerometer, scale factor and misposition are distinguishable.

Single Axis Rate-Gyroscope Error Model

Each projectile also has three single axis rate gyroscopes that are rigidly mounted the projectile. Individual gyroscope reference frames are related to the body frame by:

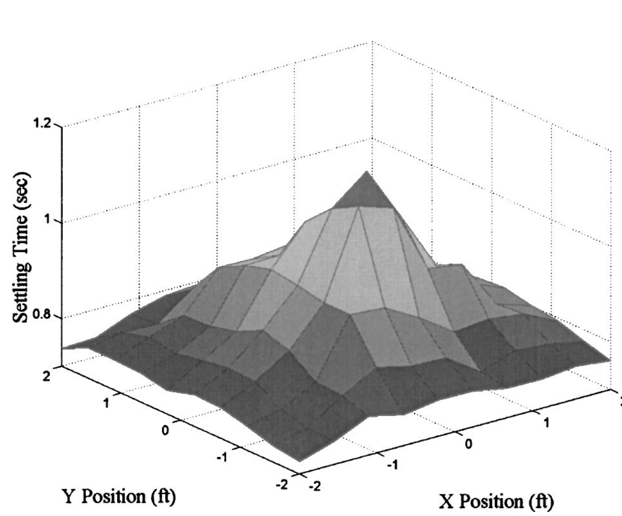

Fig. 20 Accelerometer Scale Factor Parameter Settling Time vs. Projectile Mounting Position.

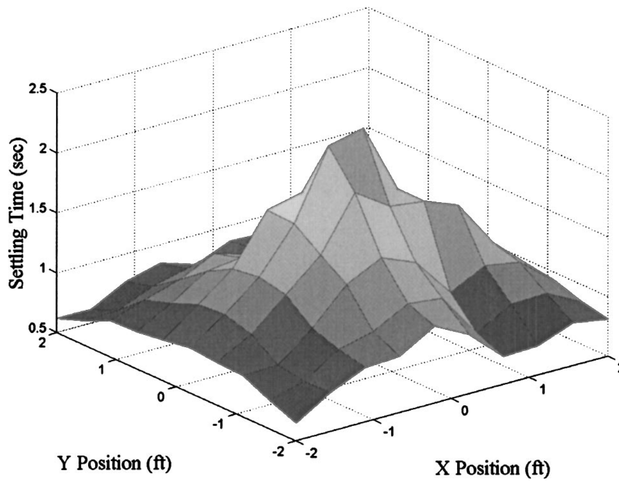

Fig. 21 Accelerometer Bias Parameter Settling Time vs. Projectile Mounting Position.

$$\begin{Bmatrix} \overline{I}_{S_i} \\ \overline{J}_{S_i} \\ \overline{K}_{S_i} \end{Bmatrix} = [T_{G_i}] \begin{Bmatrix} \overline{I}_B \\ \overline{J}_B \\ \overline{K}_B \end{Bmatrix} \tag{20}$$

The angular velocity of the i[th] gyroscope expressed in the i[th] gyroscope reference frame is given by:

$$\begin{Bmatrix} \omega_{x_i} \\ \omega_{y_i} \\ \omega_{z_i} \end{Bmatrix} = [T_{G_i}] \begin{Bmatrix} p_B \\ q_B \\ r_B \end{Bmatrix} \tag{21}$$

The true rotation rates are corrupted by noise, bias errors, scale factor error, and cross axis sensitivity.

$$\omega_i = \omega_{N_i} + \omega_{B_i} + [S_{G_i} \;\; C^y_{G_i} \;\; C^z_{G_i}][T_{G_i}] \begin{Bmatrix} p_B \\ q_B \\ r_B \end{Bmatrix} \tag{22}$$

Kalman Filter Estimation

Many approaches are available for parameter estimation problems. These methods can generally be split into two types: batch and recursive. In the case of a batch estimator of calibration parameters, a calibration test is executed and all measurements are recorded and stored. After the test is complete, calibration parameters are computed using the entire data set. In a batch estimator, all measured data is first stored and then processed. For large streams of measurement data, this requires manipulation and evaluation of large matrices and vectors. With a recursive estimator, computation of the calibration parameters evolves as new measurement data is introduced. In a recursive estimator, the entire set of measurement data does not need to be stored and manipulating and evaluating large matrices and vectors is avoided. A recursive estimator is well suited to real-time environment since estimation of calibration constants evolves as measurement data becomes available. It is then possible to monitor convergence of the calibration parameters, thus enabling excitation of the system until acceptable convergence of the calibration parameters is achieved. Kalman filtering (KF) is a widely used recursive method to estimate the state of a linear system at a given instant in time using measurements that are linearly related to the states and corrupted by noise [11]. A Kalman Filter minimizes the square of the estimation error when measurement noise is Gaussian. It can also be used in non-linear systems using the extended Kalman filter (EKF) [12]. The Kalman filter is an iterative routine which begins with an initial estimate of the state and corresponding covariance matrix. The state and covariance matrix are extrapolated forward in time using an analytic model of the system. Using measurement data, the Kalman filter gain is computed, and a new estimate of the state is calculated. Due to the fact that the error parameter model is nonlinear, a batch processing technique is not suitable.

The calibration parameters to be estimated are the following constants: accelerometer bias (3 constants), accelerometer scale factor (3 constants), accelerometer cross axis sensitivity (6 constants), accelerometer misposition (9 constants), gyroscope bias (3 constants), gyroscope scale factor (3 constants), and gyroscope cross axis sensitivity (6 constants). Evolution of the 33 calibration constants to be estimated can be cast in the form:

$$\tilde{x}_k = A\tilde{x}_{k-1} + Bu_{k-1} \tag{23}$$

where: $A=[I]$, $B=[0]$. The measurement model $c_k(\tilde{x}_k)$ is given by the expansion of Eqs. (17) and (22).

$$\tilde{z}_k = c_k(\tilde{x}_k) \tag{24}$$

$$\tilde{z}_k = [a_1 \;\; a_2 \;\; a_3 \;\; \omega_1 \;\; \omega_2 \;\; \omega_3]^T \tag{25}$$

Since the KF is an optimal linear estimator, the above nonlinear measurement model $c_k(\tilde{x}_k)$ is linearized leading to the discrete EKF.

$$C_k = \left.\frac{\partial c_k}{\partial x}\right|_{x=\tilde{x}_{k-1}} \tag{26}$$

In general, evolution of the covariance matrix is governed by the equation:

$$P_k = AP_{k-1}A^T + Q_{k-1} \tag{27}$$

which simplifies to:

$$P_k = P_{k-1} \tag{28}$$

when estimating constants. When new measurement data becomes available, the states are updated from:

$$\tilde{x}_k = \tilde{x}_{k-1} + K_k(z_k - \tilde{z}_k) \tag{29}$$

where the Kalman gain, K_k, is the factor used to weight the current measurement in the state estimate routine:

$$K_k = P_k C_k^T [C_k P_k C_k^T + R_k]^{-1} \tag{30}$$

The covariance matrix corresponding to the current state estimate is then updated. Shown below is the Joseph form for the covariance matrix update.

$$P_k = (I - K_k C_k) P_{k-1} (I - K_k C_k)^T + K_k R K_k^T \tag{31}$$

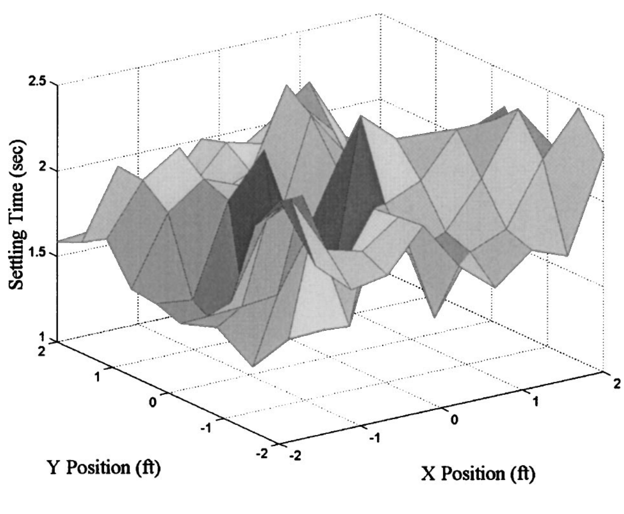

Fig. 22 Accelerometer Misposition Parameter Settlign Time vs. Projectile Mounting Position.

The dynamic platform simulation provides the corrupted readings ($\tilde{z}_k$) and the non-corrupted values (z_k). The measurement model (C_k) is obtained by linearizing Eqs. (17) and (22). Having these, Eqs. (30) and (31) provide a means for calculating the Kalman gain and determining a new estimate of the calibration parameters. This iterative process is repeated at each time step.

Results

IMU sensor calibration for a single bullet was investigated with the following error parameters considered: accelerometer and gyroscope scale factor, bias, cross axis sensitivity along with accelerometer misposition. Figures 2–14 show time simulation data and the calibration parameter estimation dynamics for a nominal case. For the nominal case the size of the table is 4 ft. by 4 ft. and weighs 200 lbs. The four spring and damper coefficients are uniformly set to 65 lbf/ft and 0.3 lbf sec/ft respectively. A single 40-mm round is located at $\vec{r}_{P\to\oplus}=[1.0\ 1.0\ 0.2]^T$ and is rotated 45° about $\underline{J_B}$ and 45° about $\underline{I_B}$ so as to excite each accelerometer with roughly the same acceleration magnitude. For Figs. 2–21 sensor data was sampled at 1000 Hz for Kalman filter measurement data input.

A schematic of the table is shown in Fig. 1. The pitch angle of the table oscillates through more than 80 degrees initially at a frequency of approximately 1 Hz. The table roll angle is initially -20 degrees and experiences damped vibration, also at a frequency of approximately 1 Hz. The yaw angle of the table begins at 20 degrees and wonders between 20 degrees and -10 degrees through the event. The angular rates of the table in Fig. 3 show the rates remain under 6 rad/sec. Figures 4 and 5 show representative accelerometer and gyroscope readings with sensor calibration error and noise compared to perfect acceleration and angular rate quantities. Although sensor errors are relatively small compared to the signal, when used as part of an IMU, the accelerometer measurements are integrated twice to obtain position and the gyroscope data is integrated once to obtain body orientation angles. Seemingly small errors in the measurement data propagate quickly into large position/orientation errors when integrated inside an IMU.

Figures 6–14 show the estimation dynamics of the projectile calibration parameters. A total of 33 calibration constants are estimated. In an ideal sensor system, bias and cross axis sensitivity equal zero and scale factor equals one. Also, in an ideal sensor system, the sensors are mounted exactly in the correct location on the body. Calibration constants are initially set to ideal values. All parameters converge to 1% of their actual value within 2.5 seconds and most converge much more rapidly. Accelerometer cross axis sensitivity values are largely converged within 0.6 seconds while the gyroscope cross axis sensitivity values are converged within 1.5 seconds. Scale Factor estimates converge within 1.5 seconds for both accelerometers and gyroscopes. Accelerometer misplacement requires the longest time to converge, as shown in Figures 8–10. Accelerometer bias converges within 1 second (Fig. 11), while the gyroscope bias converges in 0.5 seconds (Fig. 14).

In order to understand how specific table characteristics affect the performance of the estimation process, several parametric studies were conducted including varying support stiffness and damping, magnitude of initial motion, and projectile position on the table. Figures 15 and 16 show the settling time of the accelerometer and gyroscope parameters respectively as a function of spring stiffness. In this case, damping of the corner supports is set to zero and the corner support stiffnesses are equal. For each support stiffness, many simulations were performed by varying the initial orientation of the table from an initially quiescent state. The initial orientation angles were modeled as independent guassian random variables with zero mean and a standard deviation of 25 degrees. All calibration parameter settling times rapidly decay to constant values as a function of support stiffness except accelerometer misposition. Accelerometer misposition settling time is minimized near a uniform spring stiffness of 65 lb/ft. Since the settling time for the accelerometer misposition parameters is the largest, these parameters drive the performance of the calibration table.

Although not shown in figure form, support damping has little effect on convergence of any calibration parameters except accelerometer misposition. Accelerometer misposition settling time is minimized when damping is zero. Accelerometer misplacement converges quickest when the stiffness on each support is equal.

Figures 17 and 18 investigate the effect of the initial magnitude of motion, as measured by the total initial angular deflection of the table, on the settling time performance. For these cases, support stiffness and damping coefficients are held constant at 65 lbf/ft and 0 lbf sec/ft respectively. As the magnitude of initial motion is increased, settling time rapidly drops off. However, around 20 degrees of initial angular displacement a point of diminishing returns is experienced as the settling time levels off.

Figures 19–22 examine the effects of bullet placement on the table on calibration parameter settling time. The calibration table is loaded with 100 bullets evenly distributed across its surface. Accelerometer cross axis sensitivity, scale factor and bias parameter settling times are minimized as bullet placement moves away from the center of the table. However, accelerometer misplacement parameter settling time is unaffected by table placement position. Since accelerometer misplacement settling time is generally the largest, bullet position does not affect total calibration settling time.

Conclusions

It is possible to utilize a simple free vibrating platform with projectiles rigidly mounted to determine a range of calibration parameters for accelerometers and gyroscopes that are part of projectile sensor suites. This technique should be helpful to smart projectile manufacturers seeking to minimize total design cost of each round and permit high volume manufacturing lines. Settling time of calibration parameters is sensitive to corner support stiffness but largely insensitive to corner support damping. The minimum settling time is achieved when the corner support stiffness' are equal and the damping is zero. The settling time is relatively unaffected by projectile mounting location, permitting use of the complete calibration table surface. Accelerometer misposition calibration constant estimation generally requires the longest time to settle and as such drives the overall performance of the calibration device. Settling time of the calibration parameters is a strong function of the initial magnitude of motion and shows a rapidly decreasing trend.

Nomenclature

ϕ,θ,ψ = Euler roll, pitch and yaw table orientation angles
p,q,r = angular velocity of table with respect to the ground expressed in the table reference frame
L,M,N = total applied moment on the table about the table mass center
x_k = parameter estimation state vector at the k^{th} computation step
z_k = parameter estimation measurement vector at the k^{th} computation step
K_k = parameter estimation Kalman filter gain matrix at the k^{th} computation step
c = parameter estimation measurement model
C_k = parameter estimation linearized measurement matrix at the k^{th} computation step
I = mass moment of inertia matrix of the table about the table reference frame
A_k = parameter estimation state transition matrix at the k^{th} computation step
P_k = parameter estimation error covariance matrix at the k^{th} computation step

R_k = parameter estimation standard deviation of measurement noise at the k^th computation step
T_{G_i} = transformation matrix from body reference frame to the i^th gyroscope reference frame
s_i^G = scale factor of the i^th gyroscope
c_{iy}^G = cross axis sensitivity of the i^th gyroscope with respect to the $\overline{J}_{G_i}$ axis
c_{iz}^G = cross axis sensitivity of the i^th gyroscope with respect to the $\overline{K}_{G_i}$ axis
ω_{B_i} = bias of i^th gyroscope
ω_{N_i} = noise of i^th gyroscope
T_{A_i} = transformation matrix from body reference frame to the i^th accelerometer reference frame
s_i^A = scale factor of the i^th accelerometer
c_{iy}^A = cross axis sensitivity of the i^th accelerometer with respect to the $\overline{J}_{A_i}$ axis
c_{iy}^A = cross axis sensitivity of the i^th accelerometer with respect to the $\overline{K}_{A_i}$ axis
a_{B_i} = bias of i^th accelerometer
a_{N_i} = noise of i^th accelerometer
$\vec{r}_{P\to\oplus}$ = distance vector from pivot point of table to mass center of a projectile
$\vec{r}_{\oplus\to s_i}$ = distance vector from mass center of a projectile to specified sensor
$\Delta\vec{r}_{error}$ = error in distance vector from projectile mass center to specified sensor
$\vec{r}_{\oplus\to f_i}$ = distance vector from mass center to i^th floor point spring connection (I frame)
$\vec{r}_{\oplus\to c_i}$ = distance vector from the table mass center to i^th table support
k_i = spring constant of the i^th support
c_i = damping coefficient of the i^th support
$\vec{r}_{P\to\oplus}$ = distance vector from table pivot point to table mass center

References

[1] Tustin, W., 1987, ''How to Calibrate Accelerometer Systems,'' Evaluation Engineering, **26**, pp. 68–73.
[2] McConnell, K. G., and Han, S. B., 1991, ''A Theoretical Basis for Cross-Axis Corrections in Tri-Axial Accelerometers,'' *Proceedings of the International Modal Analysis Conference*, Vol. 1, pp. 171–175.
[3] Witter, M. C., and Brown, D. L., 1998, ''Broadband 6 DOF Accelerometer Calibration Via Impact Excitation,'' *Proceedings of the* 16*th* *International Modal Analysis Conference*, Vol. 2, pp. 907–914.
[4] Boutillon, X., and Faure, C., 1998, ''The Mean-Projection Method for the Transverse Calibration of Accelerometers,'' Acustica United, **84**(2), pp. 348–358.
[5] Sutton, C. M., 1990, ''Accelerometer Calibration by Dynamic Position Measurement Using Heterodyne Laser Interferometry,'' Metrologia, **27**, pp. 133–138.
[6] Payne, B., and Evans, D. J., 1999, ''Comparison of Results of Calibrating the Magnitude of the Sensitivity of Accelerometers by Laser Interferometry and Reciprocity,'' Metrologia, **36**, pp. 391–394.
[7] Gabrielson, T. B., 1997, ''Free-Mass Reciprocity Calibration,'' J. Acoust. Soc. Am., **102**, pp. 2800–2808.
[8] Grewal, M. S., 1991, ''Application of Kalman filtering to the Calibration and Alignment of Inertial Navigation Systems,'' IEEE Trans. Autom. Control, **36**(1), pp. 4–12.
[9] Kong, X., Nebot, E. M., and Durrant-Whyte, H., 1999, ''Development of a Non-Linear Psi-Angle Model for Large Misalignment Errors and its Application is INS Alignment and Calibration,'' *Proceedings of the 1999 IEEE International Conference on Robotics & Automation*, Vol. 2, pp. 1430–1435.
[10] Ginsberg, J. H., 1995, *Advanced Engineering Dynamics*, Second Edition, Cambridge University Press, New York, New York, ISBN 0521-47021-8.
[11] Grewal, M. S., and Andrews, A. P., 2001, *Kalman Filtering Theory and Practice Using MATLAB*, John Wiley & Sons, United States, pp. 114–164.
[12] Grewal, M. S., and Andrews, A. P., 2001, *Kalman Filtering Theory and Practice Using MATLAB*, John Wiley & Sons, United States, pp. 169–199.